OBSERVATIONS AND MODEL SIMULATION OF AgI SEEDING WITHIN A WINTER STORM OVER UTAH'S WASATCH PLATEAU

Edmond W. Holroyd III[a], James A. Heimbach[b] and Arlin B. Super[a]

[a] Bureau of Reclamation, Denver CO
[b] University of North Carolina at Asheville NC

Abstract. Observations from a cloud seeding experiment conducted over the Wasatch Plateau of central Utah were analyzed for treatment effect and were modeled. The day was characterized by weak surface winds, light snowfall and weak convection embedded in a thin orographic cloud during the final stages of a storm. Silver iodide was released from a generator well up the windward (west) slope of the Plateau. Seeded periods and locations were defined using measurements of co-released SF_6 tracer gas and a drifting frame of reference. Seeded and nonseeded periods and domains were defined using the derived plume history. A strong seeding signal was found in the occurrence of ice particles, both on the Plateau top and at aircraft levels. Calculations based on van-mounted 2D-C probe observations along the Plateau top's west edge indicated increased snowfall rates in the silver iodide plume, primarily due to aggregates. While some precipitation gauge observations farther downwind suggested possible increased snowfall, the evidence was not definitive and any seeding-caused snowfall was quite limited in amount. Application of the Clark mesoscale numerical model suggested the case was characterized by weak and shallow clouds principally driven by orographic influences with little buoyant contribution. The simulated tracer and cloud patterns were associated with orographic lifting and gravity waves. The model correctly predicted plume transport from the release point over the target area, but at a slower rate than indicated by field measurements. The plume core was predicted to be transported over the Radar-Radiometer site and somewhat south of the Target site to a height of about 1 km above the Plateau in good agreement with observations.

1. INTRODUCTION

The National Oceanic and Atmospheric Administration (NOAA) administers the Atmospheric Modification Program (AMP) in cooperation with the States of Arizona, Illinois, Nevada, North Dakota, Texas and Utah. The overall goals of the Utah/NOAA AMP are to physically evaluate the operational seeding program that has been conducted in Utah for over two decades (Griffith et al. 1991), and to suggest ways of improving the program's effectiveness. Toward those objectives, the Utah/NOAA AMP conducted a field program on the Wasatch Plateau (hereafter Plateau) of central Utah from mid-January to mid-March 1994. A similar field program was conducted at the same place in early 1991. Papers describing results from the 1991 program include Griffith et al. (1992), Heimbach and Hall (1994), Super (1994), Super and Holroyd (1994), Huggins (1995), and Super (1995).

This paper examines a silver iodide (AgI) seeding experiment conducted on 21 February 1994 during a period with thin (1 km thick) orographic cloud and weak embedded convection in flow from the southwest near the end of a storm episode. This experiment was selected for a detailed case study because a good observational data set was obtained and obvious microphysical changes resulted from the AgI seeding. However, it will be shown that both supercooled liquid water (SLW) and snowfall were limited during the experiment. Similar low SLW amounts and precipitation rates are typical of many winter storm hours (Super 1994). Microphysical effects of seeding were pronounced both on the Plateau top and at aircraft levels. Ground-released plumes were well observed and good supporting data were obtained. Consequently, the experiment was selected for intensive case study analysis and simulation by numerical modeling. The combination of a high quality observational set and sophisticated modeling offers a powerful approach toward improved understanding of seeding plume transport and dispersion and associated microphysical effects within orographic clouds.

Silver iodide and sulfur hexafluoride (SF_6) tracer gas were released from the Aspen Hills Site (AHS) located well up the west (windward) slope of the Plateau at an elevation of 2340 m (all elevation and altitude references will be above mean sea level). The valley floor was at about 1800 m and the Plateau was at about 2900 m. Various instrument sites used in early 1994 are shown on Fig. 1. Aircraft sampling was done with the NOAA Beechcraft King Air C-90 along the two flight tracks ("west track" and "east track") shown on Fig. 1, and also along a line connecting the radar-radiometer site (RRS, elevation 2980 m) and target site (TAR, elevation 2900 m). Instrumented van sampling of AgI ice nuclei (IN), SF_6, and ice particles was done primarily along the "upwind highway", a section of Highway 31 from its intersection with Highway 264 to southeast (SE) of RRS. The upwind highway north of RRS is essentially under the west flight track. Some van sampling was done from the same intersection to near TAR and back along Highway 264.

The main observations to be discussed include AgI IN measured by four NCAR acoustical IN counters (hereafter NCAR IN counters) (Langer, 1973) in the aircraft, van, RRS and TAR. A recent comparison has shown reasonable agreement between the van and aircraft NCAR IN counters and the Colorado State University isothermal cloud chamber (DeMott et al., 1995). Concentrations of SF_6 were measured with fast-response detectors (Benner and Lamb, 1985) in the aircraft and van. Ice particles were detected by Particle Measuring Systems (PMS) 2D-C imaging probes on the aircraft and van, and at TAR. The latter two probes were vane-mounted which kept them pointed into the resultant wind.

Rawinsonde observations were obtained from site RAW in the valley west of the Plateau. Wind speed and direction, temperature, relative humidity (or dewpoint temperature) and precipitation were measured at several surface locations shown on Fig. 1. Winds, positioning and state variables were measured by the aircraft. Supercooled liquid water was monitored by a vertical-pointed microwave radiometer (Hogg et al. 1983) at RRS, by Rosemount icing rate meters at HAS, RRS and TAR, and by a King liquid water probe on the aircraft. K_a-band radar volume scans were made from RRS. A Doppler acoustic sounder (sodar) observed half-hourly averaged horizontal winds over DAS.

2. SYNOPTIC CONDITIONS

There was a long wave trough over the western continental United States. One of several short wave troughs embedded within this feature passed over Utah in the early morning of 21 February. A stationary front extended from northern Idaho through southern Wyoming, through eastern Colorado and northern New Mexico. In the early morning, a fast-moving storm system associated with the upper short wave trough passed to the south of the Plateau. Most sections of Utah received some snow with the heaviest snowfalls over the mountains and higher southeast valleys. Some mountainous areas received 15 to 25 cm of snow during the night. The experiment was conducted in the morning after the passage of the surface trough. During the experiment the target area had weak convective precipitation stimulated by orography while the valleys had broken clouds.

3. THERMODYNAMICS

Vertical profiles of potential and equivalent potential temperature were made from rawinsonde, aircraft, and surface data. From the valley floor at 1800 m to 4000 m the potential temperature increased from about 287°K to about 292°K, though the range at surface sites was 285 to 297°K caused in part by solar heating. The profile indicates that the air was somewhat stable with respect to the dry adiabatic lapse rate, though solar heating could easily create local instabilities. Such instabilities may have helped the seeding plumes rise more rapidly on thermally driven updrafts than would have been the case with purely mechanical mixing as was simulated by the model described later. Studies on the Grand Mesa, Colorado, (Holroyd et al. 1988) showed that surface air could rise (bringing nuclei with it) in otherwise stable air to the level at which the ambient potential temperature equalled the peak found at the surface.

Profiles of equivalent potential temperature decreased slightly from about 296.5°K in the valley to about 293.5°K aloft. Surface stations ranged from 287 to 306°K. The air was therefore slightly conditionally unstable, mostly because dew points decreased with altitude. Convective elements could rise easily but mixing would dry and dissipate them. Broken convective cloudiness was in fact observed over the Sanpete Valley throughout the experiment. Cloud cover was generally solid over

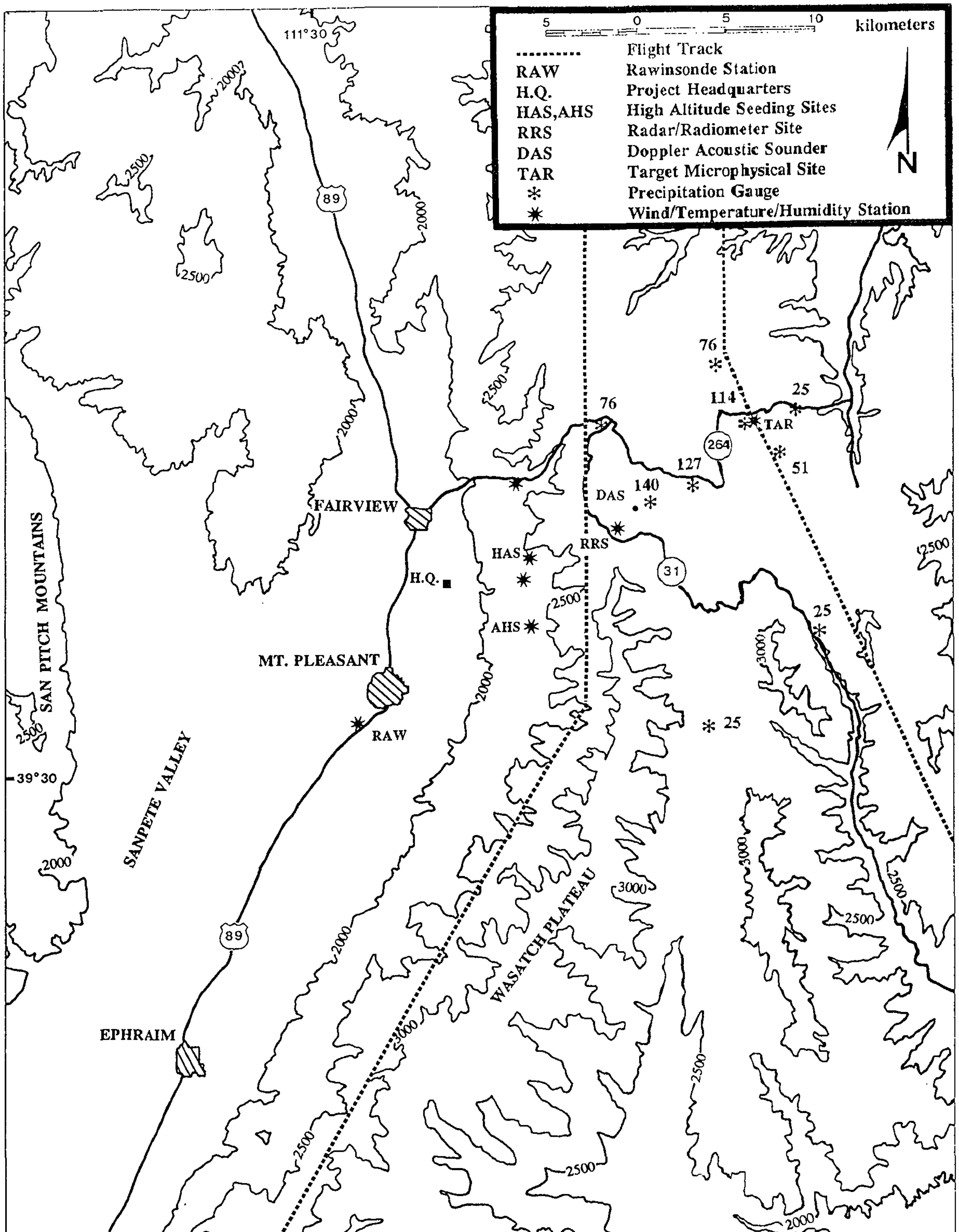

*Fig. 1. Map of the Wasatch Plateau experimental area showing equipment siting and highways used for the early 1994 field program. The two dashed lines are aircraft sampling tracks over the west and east edges of the Plateau top. Contours are in meters above mean sea level. Numbers by the nine gauges represent total precipitation (mm * 100) received after estimated AgI plume arrival (see text).*

the Plateau at the beginning of the experiment, but was becoming broken by the end.

4. PLUME DETERMINATION

Silver iodide was released from AHS from 0800 to 1215 (all times local standard) at 22.5 g h^{-1} (a typical ground release rate) with a Desert Research Institute radio-controlled generator. Sulfur hexafluoride was released from 0830 to 1212. The stated times, together with wind speed and direction, determined the extents of the plumes along the wind direction axis. Diffusion, deflection, and wind variability determined the transverse extents relative to the mean wind direction axis. Wind directions over the Plateau were generally from the southwest. Wind speeds over the Plateau were faster than over the valley at the same pressure altitude.

4.1 Drift Speed

A distinct but small wind shift to more southerly directions was detected in the data from the AHS and HAS (0950-1020), RRS (1012-1036), and TAR (1055-1115) sites. The wind shift was accompanied by an marked increase in detected IN at the RRS and TAR sites and warmer air temperatures. A restoration of original wind directions followed. A drift speed of 4.5 ± 1 m s^{-1} was calculated by tracking the fluctuations of IN, temperature, and winds between all four sites. This abnormally slow speed is within or near the scatter of those calculated from aircraft straight-and-level flight segments (6 ± 3 m s^{-1}) and from well-exposed Plateau top surface instruments ($3.7 \pm .9$ at RRS to 5.8 ± 1.1 m s^{-1} at TAR). Wind speeds at RAW, in the upwind canyons, and at the two west slope seeding sites (AHS and the unused HAS) were slower.

4.2 Drift Direction

The plume positions were readily determined by the boundaries of enhanced concentrations of SF_6, AgI, and ice particles, as recorded by the aircraft, van, and surface instruments at RRS and TAR. The angle from the plume center back to the AHS release site was calculated to give the drift direction of the plume. Aircraft observations showed plume orientations near 235 degrees for the first passes along the west track, 235 degrees for the lower passes along the east track, 244 and 253 degrees for the top two east track passes, and 243 degrees for the last west track passes. Vertical shear existed over the east track but not the west track. The winds were becoming more westerly with time along the west track. The van found plume orientations of about 240 degrees before and after the more southerly wind shift and 227 degrees during it.

These directions of plume transport are close to the winds determined by the 0900 RAW rawinsonde for the same altitudes but with the expected more southerly shift caused by friction over the Plateau. The constriction of the air flow caused by the height of the Plateau was responsible for the increased wind speeds there. The lack of wind shear over the west track may indicate that most of the air at the levels of the experiment came from a common source (Sanpete Valley) and had a common momentum. Its forced rise dominated wind speed and direction near the RRS. Farther downwind, near TAR, the air had time to respond to normal pressure gradients and showed angular shear.

4.3 Drifting Frame of Reference

A rotated coordinate system drifting with the plume was designed to refine examinations of the plume behavior. The new frame of reference was used to coordinate the time and space differences among the many observations. The observations are thereby related to positions relative to the plume itself. The origin was defined to be at RRS at 0800 and drifting with respect to the ground at 4.44 m s^{-1} (16 km h^{-1}) from 235 degrees. The abscissa was oriented parallel to 235 degrees and is representative of time in a steady state flow. The ordinate was therefore perpendicular to the plume axis and measures diffusion and fluctuations transverse to the mean axis. The slight change in speed from the actual value of 4.5 m s^{-1} was for ease in plotting graphics and is insignificant; it amounts to a discrepancy of less than 1 km over the 4.25 hour experiment.

Figure 2 shows the plume in the rotated and drifting (new) frame of reference. The long figure is split into two pieces, a. start and b. end, with repeated center, for ease of display. Earlier times are to the right and later to the left. The AHS site ordinate was -0.94 km and the TAR ordinate was 0.97 km. The AgI IN concentrations (light shading) are plotted on a compact logarithmic scale above the drift track of the RRS and TAR sites through the figure. SF_6 concentrations are hand

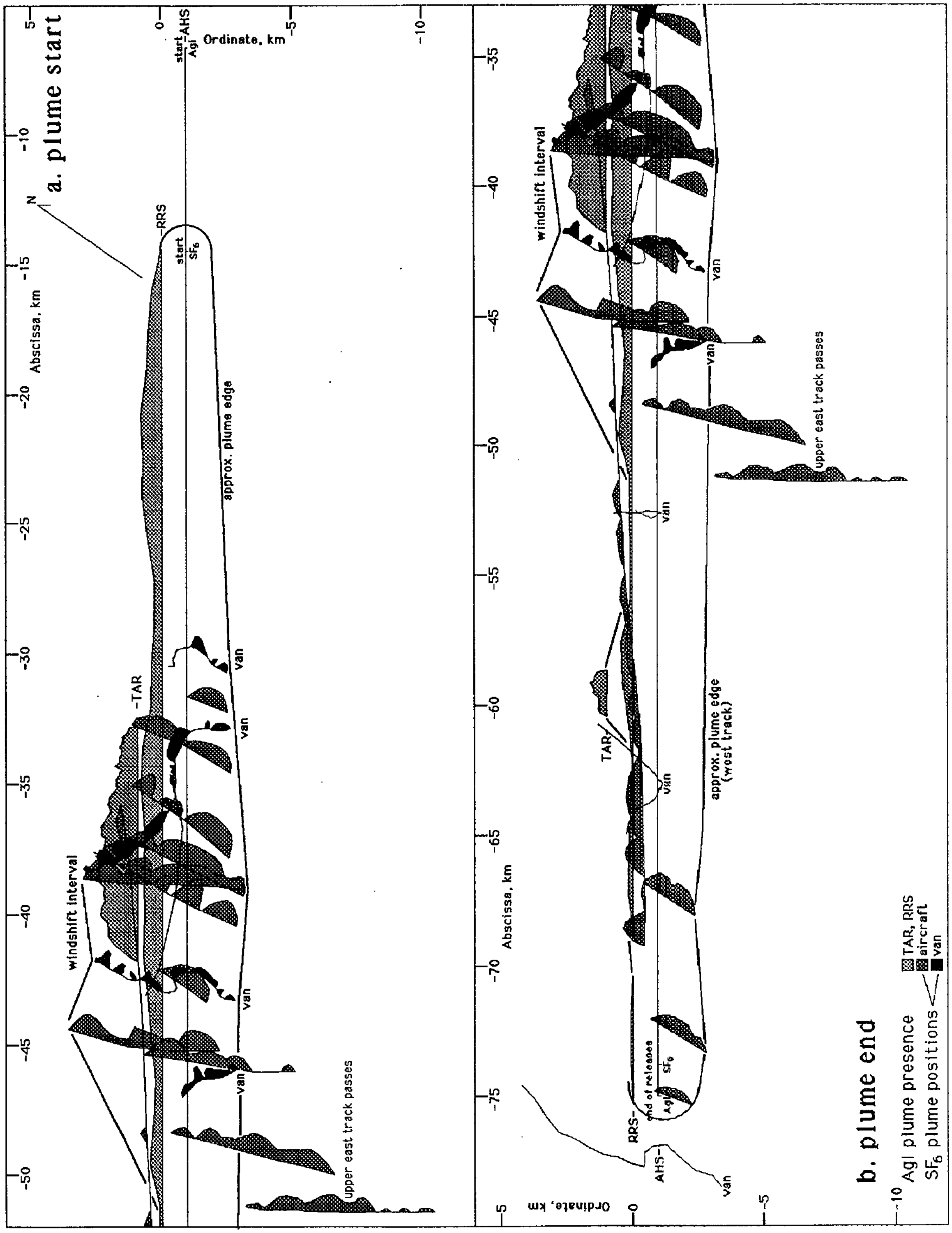

Fig. 2. The plume as defined in a coordinate system drifting from 235 degrees at 16 km h^{-1} (see text). Ground sites track leftward with time along a constant ordinate. Aircraft and van passes in the plume are indicated by thin line tracks. AgI and SF_6 concentrations are graphed with shading above or to the right of the tracks.

sketched on a similar compact logarithmic scale to the right of the tracks (thin lines) of the aircraft (medium shading) and van (dark shading). Some approximate SF_6 plume edges are suggested by the thick lines. The plume concentrations are obviously variable with position. Similar concentration graphs could have been plotted from ice particle data from the aircraft and van and from IN data from the van. Slight concentrations of IN and ice particles were measured by the east van pass at abscissa -57 and stronger concentrations on the return pass at -63, though no SF_6 was indicated in the final data (contrary to field notes). The last pass of the van (abscissa -77) found no SF_6, AgI IN, or significant ice particle concentrations, confirming the shutdown of the generators and the rapid flushing of IN from the study region.

The AgI plume length in the new frame of reference was 68 km, starting at abscissa -6.7 km (0800 release start at AHS) and ending at -74.7 km (1215 end of release). The SF_6 plume length was 59 km, starting at -14.7 km (0830 release start at AHS) and ending at -73.7 km (1112 end of release). The AgI was detected at RRS (1 km away from AHS in the new frame) as soon as the instrument was turned on at 0900, about a half hour after expected for a transport speed of 4.5 m s^{-1}. Only traces of AgI were detected at the RRS during the final hour of its expected presence.

The presence of AgI IN at TAR was detected at low levels (1-4 counts s^{-1}, equivalent to about 60-240 IN L^{-1} effective at -20°C) as soon as the data system was started at 1000. (Background IN levels in the absence of AgI, as measured with an NCAR IN counter on the Plateau, were typically 1-4 counts min^{-1}.) Similar low levels of AgI were detected throughout the experiment with two exceptions. Levels decreased to near background after 1235, and much higher levels (10-40 counts s^{-1}) were monitored between 1049 to 1111. The brief period of high AgI IN concentrations was associated with the southerly wind shift. At other times most of the plume was south of TAR.

Van and aircraft sampling of the plume did not occur until about abscissa -30 km. The SF_6 plume width then was 1.5 to 2.0 km on each of the first van (starting at 0954) and aircraft (starting at 0957) detections of the gas. Thereafter the SF_6 plume rapidly expanded to a width of 4.0 to 5.5 km with numerous internal peaks in concentrations. Those peaks appear to be associated with the positions of the canyon heads upwind. The widening of the plume was associated with the wind shift. The plume top on the east track was laterally sheared to a width of 7 km at a more southerly position. Starting with a van penetration (1058) at abscissa -46 km, the plume width along the western track shrank to a steady 2 km until the end of the experiment when plumes were no longer found along the upwind highway.

Initial examination of K_a-band radar volume scan data from the RRS did not provide definite evidence of plume position. Apparently radar returns from widespread natural snowfall obscured any returns from presumably smaller seeded ice particles because of the strong dependence of radar reflectivity on ice particle size and mass.

The typical transverse plume spread of 2 km at about the RRS site is equivalent to an angular spread of about 15 degrees. That value is comparable to seeding plumes on the Grand Mesa, Colorado, (Holroyd et al. 1988) released under similar conditions. The wider plume during the wind shift had an angle from AHS of about 50 degrees. There was no indication of additional transverse spreading between the west and east flight tracks, which matches some, but not all, earlier results from the Grand Mesa.

4.4 Vertical Cross Section-cross wind

Vertical cross sections were constructed through RRS at the 235 and 305 degree azimuths. They serve as bases for Figures 3 and 4. Terrain elevations within 4 km of the 235 degree axis were plotted as the scatter of dots. In Figure 3 the view is downwind and the terrain is restricted to the slopes between the seeding site, AHS, and the Plateau crest near RRS. The location of those sites are indicated by the white circles and enclosed crosses. In order to show possible channeling effects of the terrain, Figure 3 shows terrain departures from a plane that generally follows the western slope of the Plateau. The zeroing is arbitrary. This terrain cross section shows a major canyon head (between the major peaks), having about a 6 km width, and three or four minor canyon heads within having about 1.5 km widths.

At the top of Figure 3 are plotted SF_6 concentrations on compressed logarithmic scales for the first

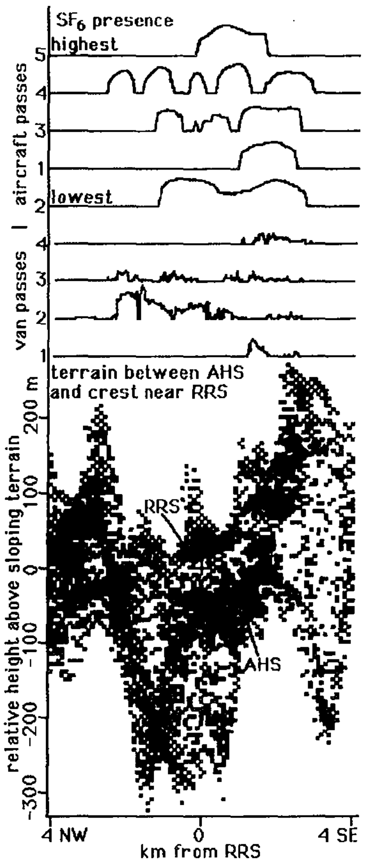

Fig. 3. A vertical cross section, looking downwind, of the terrain on the west slope of the Plateau between the seeding site, AHS, and the crest near RRS. Above are graphs of SF_6 presence as measured on some of the first passes by the van and aircraft. The canyon heads appear to affect the locations of plume maxima and extents.

Table 1. Peak SF_6 concentrations (ppt) for the aircraft and van passes of Fig. 3.

passes	peaks, left to right
aircraft-5	214
aircraft-4	25, 58, 14, 129, 18
aircraft-3	17, 5, 33
aircraft-1	65
aircraft-2	83, 56
van-4	17
van-3	17
van-2	301
van-1	40

4 van passes and the first 5 aircraft passes along the crest. Peak concentrations, in parts per trillion (ppt) by volume are given in Table 1. The scales differ somewhat between the van and the aircraft, but the graphs are intended to show mainly the plume position and structure with respect to the ground. The aircraft passes are plotted in order of their elevation.

It appears that the plume positioning and lateral spreading of the lower parts of the plume were largely controlled by the interaction of the wind direction with the topography of the canyon heads. The transverse structure of the plumes appeared to have higher concentrations aligned with the positions at which the rising air exited the minor canyons and crossed the Plateau top. For the van passes and lower aircraft passes there is a consistent plume presence on the southeast side, bounded by the higher terrain to the right of the plume. That plume width is comparable to the size of the minor canyon head in that location. Van passes 2 and 3, affected by the wind shift, appear to be bounded on the left by the other peak of higher terrain. Aircraft pass 3 appears to be partitioned by three minor canyon heads.

4.5 Vertical Cross Section-along wind

The six parts of Fig. 4 show cross sections aligned with the wind, as viewed towards the NW. Surface and aircraft observation locations are indicated by a larger symbol. Aircraft pass numbers are given as integers in Fig. 4a only. Passes 13 and 14 were parallel to the axis of the figure and are not indicated. Van passes in the plume were near RRS and from TARSW to TAR. (All 4 and 5 letter names used in this report are for precipitation gauge locations described in section 6.) An approximate edge of the plume top is indicated for reference. Data values on aircraft passes 3, 9, and 15 were appreciably low, possibly from clear subsiding air between cloud elements, for most parameters in the six parts of this figure. Values from those passes were generally ignored in the contouring but the actual values are indicated.

Fig. 4a shows the distribution of liquid water content (LWC) as determined by the aircraft passes. The data, shown as two-place decimals, were averaged throughout the plume and to about 3 km to both sides. LWC values were slightly lower within the plume, probably from greater consumption by the enhanced ice particle concentrations there. The wettest parts of the cloud were the lower layers over the western track (crest line). The cloud dried appreciably to the east. Visual observations at TAR consistently indicated a broken cloud deck

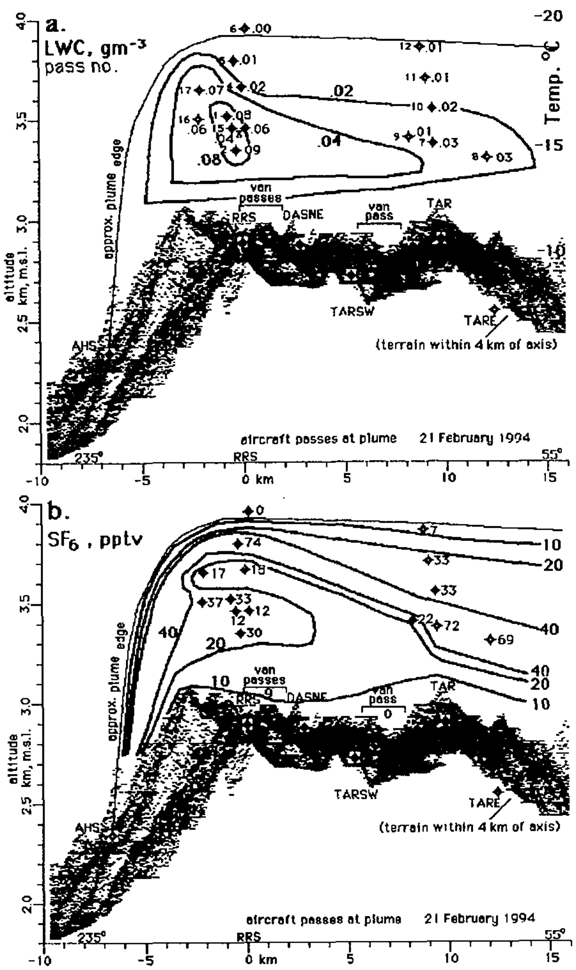

Fig. 4. Vertical cross sections, looking cross wind to the NW, of plume and microphysics parameters. The panels are a. LWC, temperature and pass number; b. SF_6, c. IN, d. ice concentration, e. nonseeded IWC, and f. seeded IWC and particle trajectories.

based well above the site from 0948 (first observation) through the experiment's end. In contrast, the RRS was in cloud until after 1200. This is further evidence of subsiding air over the Plateau top's east edge.

Temperatures, shown at the right of Fig. 4a, are generally from -11°C at the Plateau top to -19°C at cloud top. AgI is active in this temperature range, especially at the colder end. A recent calibration of a Desert Research Institute (DRI) remote-controlled AgI generator using AgI-NH_4I-acetone solution (Huggins, 1994) indicated about 10^{15} IN per gram of AgI at -12°C, the coldest temperature

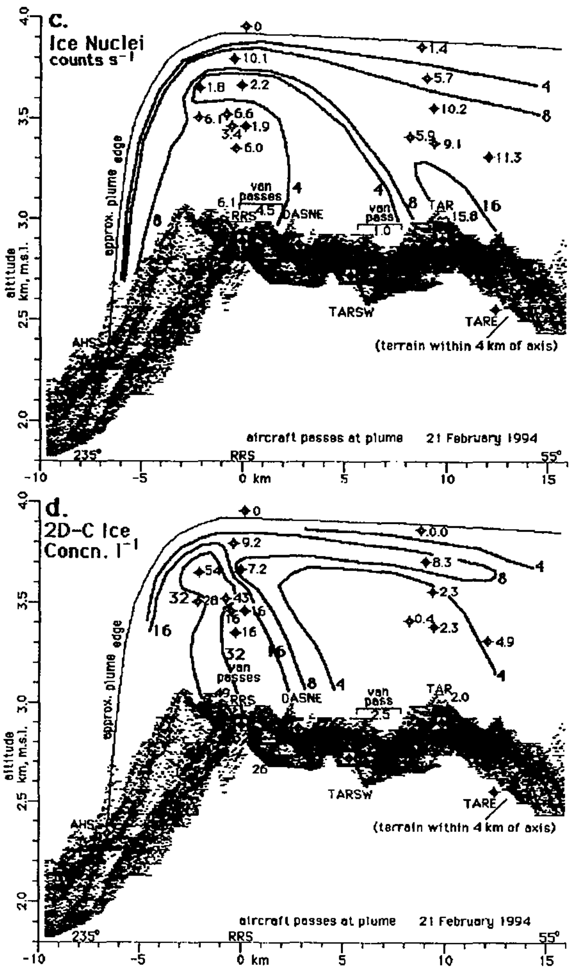

Fig. 4. (cont.), c. IN, d. ice concentration

tested, for natural draft conditions. The same type of generator and solution were used at AHS. This solution was chosen because it is used in the Utah operational seeding program.

Figures 4b, 4c, and 4d show the observed concentrations of SF_6, IN, and ice particles, respectively, averaged over the width of the SF_6 plume. NCAR IN counts were shifted by 60 s because of hold-up time in unit's cloud chamber. The SF_6 and AgI IN contours have the same basic pattern. The highest concentrations on the west flight track are at the plume top with a secondary peak at the middle levels. The highest concentrations are at the lower levels on the east track, suggesting that the plume core descended while crossing the Plateau.

At RRS (at which data were collected for 6-min periods) the IN varied considerably. They were

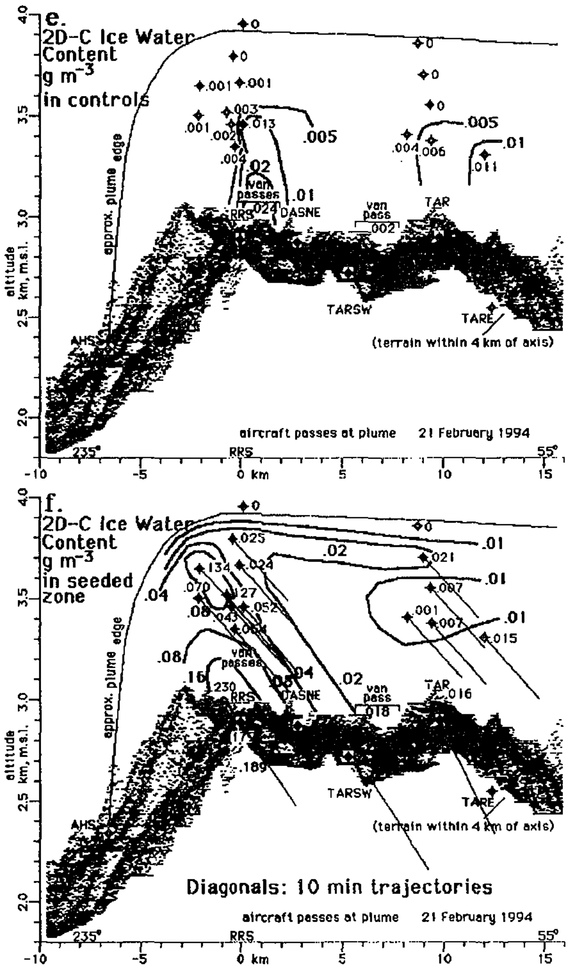

Fig. 4. (cont.), e. nonseeded IWC, and f. seeded IWC and particle trajectories.

detected in abundance from as soon as the counter was turned on at 0900 until about 0936. The wind direction was 220 to 243 degrees during this IN maximum with count rates typically near 6 counts s^{-1}. The wind shifted to between 250 to 266 degrees from 0936 until 1006 and IN levels dropped below 1 count s^{-1}. Winds at the RRS were again more southerly (226 to 241 degrees) from 1012 to 1036 and count rates showed a second maxima with values similar to the first. From 1036 through the end of the experiment the wind direction was never more southerly than 250 degrees and IN counts rates remained low. These observations indicate the AgI plume was generally south of the RRS except for the two periods with more southerly flow.

As a basis for comparison, for all RRS 6-min periods with IN averaging >1 s^{-1} the average was 6 counts s^{-1}. The TAR IN for the 35 minutes with highest concentration averaged 16 counts s^{-1}. The first four van passes along the west track were combined to an average of 4.5 counts s^{-1}. For reference, 10 counts s^{-1} is equivalent to about 600 IN per liter at -20°C, the temperature of the NCAR IN counter cloud chambers. This value results from the usual times 10 correction because of ice crystal losses to glycol-covered cloud chamber walls (Langer, 1973).

Surface IN concentrations are generally low compared to aircraft values shown in Fig. 4c. Because NCAR IN counter response times (about 60 s) are usually longer than within-plume sampling times by the aircraft, the aircraft values cited were calculated as the total counts per pass divided by the number of seconds in the SF_6 plume. In other 1991 (e.g. Super, 1995) and 1994 experiments the van values were usually much higher than aircraft values, indicating a plume core hugging the ground. This light wind case, in contrast, indicates that the SF_6 and AgI plumes were rapidly lifted to cloud top altitudes.

Fig. 4d shows a different pattern for the concentration of ice particles. The highest concentrations were observed in the middle cloud levels of the west track, particularly on the last pass. Similar high concentrations were also found by the van, plotted near RRS for three range intervals, 1 km wide, over which the four west track passes were averaged. To the east concentrations were much lower, with the greatest somewhat below cloud top. The general pattern is of rapid fallout of particles and an anvil type of remnant to the east.

Ice water contents (IWC), comparable to LWC in Fig. 4a, were calculated from the 2D-C data using concentration algorithms and masses in Holroyd (1987). They are plotted in Fig. 4e for plume nonseeded zones defined in the next section, and in Fig. 4f for measurements within the SF_6 plume (seeded zone). IWC for the nonseeded zones was everywhere less than LWC, indicating an inefficiency in the natural precipitation process. IWC for the seeded zones generally was comparable with LWC for the same intervals (the LWC in the seeded zones was somewhat reduced compared to nonseeded zones). IWC was in significant excess of LWC on passes 1 and 17 in the upper left part of

Table 2. Ice particle concentrations L^{-1}, in the seeded and nonseeded zones. (NN=north nonseeded, S=seeded, SN=south nonseeded, AN=average nonseeded, R=S/AN). Values between 0 and 0.1 indicated by >.0.

		Concentrations, L^{-1}					Precip. Rates mm h^{-1}*100				
pass	track	NN	S	SN	AN	R	NN	S	SN	AN	R
Van											
1	W	2.2	27.8	3.1	2.6	10.5	2.1	47.2	5.9	4.0	11.8
2	W	4.1	60.0	5.4	4.7	12.7	3.8	58.5	10.5	7.2	8.1
3	W	3.9	24.2	2.6	3.3	7.4	4.5	34.2	2.8	3.7	9.4
4	W	6.3	21.1	3.3	4.8	4.3	6.1	38.4	4.5	5.3	7.3
6	E	0.3	2.5	-	0.3	9.1	0.3	4.1	-	0.3	13.4
TAR	E		2.0					4.7			
Aircraft											
1	W	0.5	42.8	1.3	0.9	47.9	0.2	20.6	0.8	0.5	44.7
2	W	0.9	16.1	1.1	1.0	15.8	0.5	8.7	0.8	0.6	13.6
3	W	7.1	15.9	0.2	3.6	4.4	3.8	9.7	0.1	2.0	4.9
4	W	0	7.2	0.4	0.2	36.2	0	3.6	0.3	0.1	28.3
5	W	0	9.2	0	0	INF	0	3.8	0	0	INF
6	W	0	0	0	0	-	0	0	0	0	-
7	E	1.3	2.3	2.2	1.8	1.3	0.7	1.0	1.3	1.0	1.0
8	E	2.3	4.9	4.0	3.2	1.6	1.4	2.2	1.9	1.6	1.4
9	E	>.0	0.4	2.3	1.1	0.3	>.0	0.1	1.4	0.7	0.2
10	E	0.2	2.3	0.2	0.2	10.3	0.1	1.1	0.1	0.1	16.8
11	E	0	8.3	0	0	INF	0	3.1	0	0	INF
12	E	0	>.0	0	0	INF	0	>.0	0	0	INF
13	NE	>.0	6.6	0	>.0	671.6	>.0	3.3	0	>.0	1257.
14	NE	0	3.0	1.0	0.5	6.2	0	1.5	0.5	0.2	6.1
15	W	0.7	16.2	0.3	0.5	33.1	0.5	6.4	0.2	0.4	17.1
16	W	0.2	27.9	0.5	0.4	74.9	0.1	10.6	0.2	0.2	58.0
17	W	0	54.1	0.8	0.4	139.9	0	19.4	0.3	0.2	119.7

the figure, where the greatest ice concentration was found.

Precipitation rate calculations (not shown) from the 2D-C data have a pattern similar to the IWC. The sizes and terminal velocities of the particles contributing median values to the precipitation rates were determined. Using those terminal velocities, the 4.5 m s^{-1} drift speed, and ignoring vertical air motions, 10-minute subsequent trajectories were calculated for each pass and are shown as the diagonal lines in Fig. 4f. Half of the precipitation falls faster and half slower than indicated by these lines. The patterns along with IWC or ice particle concentrations indicate that the western track ice particles were precipitating rapidly, with much of the snowfall likely reaching the ground before the DASNE and TARSW gauges. The figures suggest that little snow would be left for the gauges near the east track.

5. ICE PARTICLE CHARACTERISTICS

5.1 Analysis of Observations

Following a procedure that has become standard for our studies, 2D-C ice particle data were analyzed by the methods discussed in Holroyd (1987) and Super et al. (1988). Ice particles less than 100 μm size (4 pixels) were ignored as were particles with estimated center of mass outside the 2D-C probe's field of view. For the van and aircraft data the seeded zone was usually defined by the entrance and exit times through the SF_6 plume. Buffer zones of 12 flight seconds for the aircraft (about 1 km) and 1 km NW or SE for the van were defined immediately adjacent to the seeded zone. Beyond that, on both sides, nonseeded (control) zones of 24 flight seconds and 2 km width were defined. Ice particle characteristics were thereby determined for five zones for each pass of the aircraft or van. The concentrations and precipitation rates from the 2D-C images are listed in Table 2 for the seeded and nonseeded zones. (Buffer zones are ignored.) Also listed are the seeded to nonseeded ratios.

The TAR site was potentially influenced by the AgI plume above it for all but the last 15 min of the 1000 to 1330 observation time period, though AgI nuclei were detected for only 35 min there. TAR data were therefore analyzed in 15 min increments and considered totally seeded. In fact, the TAR ice particle concentration showed no obvious change during the time of AgI presence.

Plume boundary exceptions are as follows: Aircraft pass 6 was in clear air; an arbitrary 1 minute period was chosen in the expected location for averaging other parameters. On the northeastward pass 13, lacking an SF_6 plume detection, the start was 44 seconds before the start of the IN detection, based on passes where both AgI and SF_6 were present. The exit time was where the ice particle concentration dropped below 1 L^{-1}. Van pass 6, returning from the target, did not have detectable SF_6 values in the processed data (contrary to field notes); the north edge plume entry was defined as 55 seconds before the average IN counts first reached 2 s^{-1}. The van penetrated further into the plume and then went back out (see Fig. 2b, abscissa -63) of the north side, which was then defined geographically. None of these variant plume edge definitions are critical to the conclusions.

It is seen that the seeded zones almost always had greatly enhanced ice particle concentrations (ratios $>>$ 1.0). That is the normal first effect of seeding shown in a number of past studies which include Holroyd et al. (1988), Super and Boe (1988), Super and Heimbach (1988), Deshler et al. (1990) and Deshler and Reynolds (1990). Precipitation rates calculated from the 2D-C images had a similar relationship. The aircraft precipitation rates are less than those measured by the van during the same time period. This is normal because ice particles have additional opportunity to grow as they fall to the ground. The rates for the van are comparable with the precipitation rates measured by gauges during the same general period shown in Table 3. The TAR 2D-C rate is much less than the average measured by the nearby TAR gauge. However, the TAR 2D-C was not operated until after 1000 and missed the more intense precipitation from 0900 to 1000. The TAR gauge detected no precipitation from 1000 until the 2D-C probe was turned off at 1330 except for 0.38 mm between 1100 to 1115. The latter interval matches a period of greater snowfall and concentrations from the TAR 2D-C from 1057 to 1127.

The ice particle size spectra for the four west track van passes were analyzed as presented in Fig. 5. Figure 5a shows the spectrum (thick lines) with respect to the particle contributions to the precipitation rate for both the seeded and nonseeded zones. Figure 5b shows the normal size spectrum of the particles with no mass or terminal velocity weighting. The basic sizes are slightly smaller for the

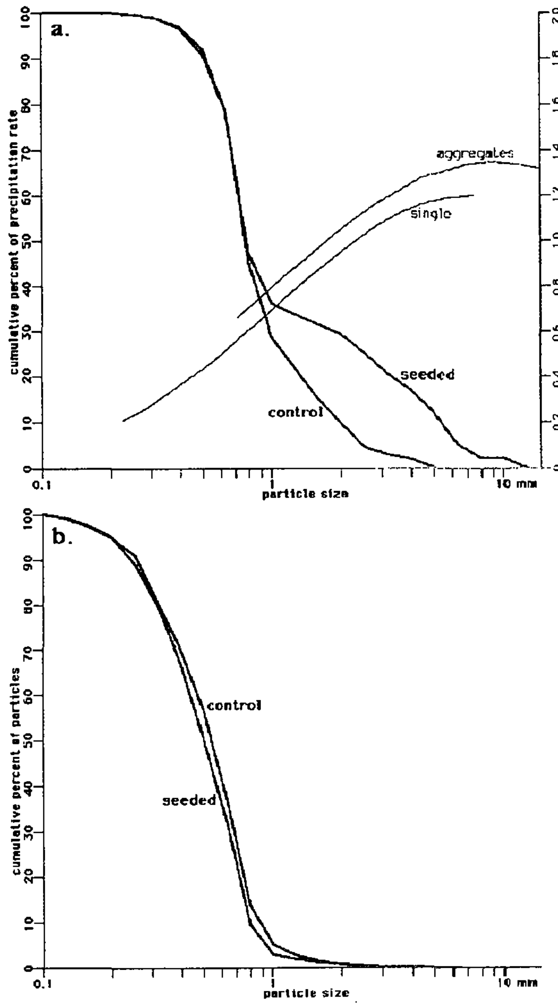

*Fig. 5. Size spectra of van 2D-C particle data. **a.** with respect to precipitation rate. **b.** with respect to particle concentration. Particle terminal velocities used for various calculations are shown in a. Aggregation accounts for the separation between the seeded and nonseeded (control) spectra in a.*

seeded zone than for the nonseeded zone except for the presence of large aggregates in the seeded zone. Those aggregates are not visible in Fig. 5b because there are about ten times as many particles (mostly small) in the seeded zone compared to the nonseeded (Table 2). Precipitation rates, however, are dominated by the large end of the particle spectrum. In the nonseeded zone the large particles are single. In the seeded zone they are aggregates of the numerous smaller particles, greatly affecting the separation of the two spectral curves in Fig. 5a. As an additional reference, the typical terminal velocities at 700 mb of the ice particles of the single particles (mostly "tiny", "hexagonal", and "irregular" classes of Holroyd 1987) and "aggregates" are shown in Fig. 5a as the thin lines. Those velocities were used in Fig. 4f.

5.2 Physical Plausibility of Apparent Seeding Effects

It is reasonable to ask whether increased aggregational growth in the AgI plume observed along the upwind highway appears physically plausible. There are two separate issues: time for nucleation of ice crystals by the AgI and time for development of aggregates greater than 1 mm size as observed within the AgI plume.

Precise cloud base observations were not available during this experiment because of failure of a time-lapse camera system at RAW. Visual observations at the RRS, located at the canyon head above AHS, noted that RRS was in cloud until between 1200 and 1230. Relative humidity measurements at AHS were about 95 percent for the first two hours of AgI release, while temperatures were -6 to -7°C. Thereafter the temperature increased and the relative humidity decreased as the storm episode ended. By 1100 the AHS temperature was -4.5°C and the relative humidity was 90 percent. Although relative humidity sensors have only moderate accuracy near water saturation, it appears likely that AHS was in-cloud until at least 1000. With temperatures colder than -6°C and humidities of at least ice saturation, rapid production of high concentrations of ice crystals can be expected very near the generator as demonstrated by the field observations of Finnegan and Pitter (1988) for the same AgI solution. Therefore, it is reasonable to assume that rapid ice crystal nucleation occurred near the AHS generator until at least 1000, and that crystals had at least 7 km of upslope transport within cloudy air before reaching the upwind highway. Winds at AHS and HAS were near 2 m s^{-1} during the experiment. Assuming a mean transport speed of 3.5 m s^{-1} from AHS to the upwind highway translates into 33 min of travel, a considerable time for crystal growth. Much less rapid ice crystal formation by contact nucleation, and less within-cloud transport, probably occurred downwind of the AHS as the cloud base presumably ascended above the seeding site sometime after 1000.

The ice crystal aggregation process is not well understood, particularly in low liquid water clouds such as sampled during this experiment. However, there is evidence in the literature to support the hypothesis that seeding can result in aggregation. For example, Holroyd and Jiusto (1971) reported that aggregation was the dominant precipitation form resulting from heavy seeding of a lake effect winter storm. Heimbach and Super (1988) presented results of observations during two storms within an AgI plume on top of the Bridger Range's main crest. These measurements, made only 3 km downwind (and upslope) from the AgI generator, showed pronounced aggregation of plates and/or linear particles. Snowcourse observations suggested marked seasonal snowpack increases only 5 km downwind of the AgI generator. Similar findings were reported for the earlier Bridger Range Experiment (Super and Heimbach 1983). Both Bridger Range studies suggested that aggregation may have produced the apparent snowpack increases within 5 km of the AgI generator.

Heymsfield (1986) reviewed evidence of aggregate development in seeded clouds and presented model calculations of the aggregation process. His views included, "The time required for the observed onset of aggregation in seeded clouds is 5 to 8 min." and "Most of the precipitation that develops in convective clouds that decay shortly after being seeded is apparently produced by aggregates." Such clouds may have limited liquid water contents typical of winter orographic clouds. Heymsfield (1986) noted that aggregation was most likely to occur at temperatures near -6 and -16°C but was unlikely between -10 and 12°C.

In view of the evidence presented, it is concluded that the van 2D-C probe observations of aggregates greater than 1 mm within the AgI plume is consistent with current physical understanding of expected seeding effects. There appears to have been adequate time for ice particle growth and aggregation in the plume of enhanced particle concentrations observed by the van along the upwind highway along the Plateau top's west edge. However, the average transport speed of 4.5 m s^{-1} on this day (Sec 4.1) was atypically slow. More typical wind speeds above the Plateau during winter storms are 2 to 3 times as fast.

6. PRECIPITATION GAUGE OBSERVATIONS

A network of precipitation gauges was operated as shown on Fig. 1. Belfort Universal weighing gauges were used with 24 h rotation chart drives

Table 3. Estimated AgI plume arrival times (HHMM), 3.5 hour precipitation totals (mm) and equivalent hourly rates (mm h^{-1}*100) at the nine precipitation gauges shown on Fig. 1. Gauges are noted as S=seeded or N=nonseeded according to whether they were under or crosswind of the AgI plume.

gauge	arrival	type	total	rate
RDJNC	0845	N	0.76	22.
TARNW	0905	N	0.76	22.
DASNE	0835	S	1.40	40.
TARSW	0845	S	1.27	36.
TAR	0900	S	1.14	33.
TARSE	0900	S	0.51	15.
TARE	0910	S	0.25	7.
FARS	0810	N	0.25	7.
FARSE	0840	N	0.25	7.

providing a time resolution of about 2 minutes. All gauges had 28.7 cm diameter orifices (twice standard area) which resulted in a snow water equivalent resolution of 0.13 mm (0.005 inch). All gauges were located in protected clearings in the conifer forest, and were equipped with Alter-type wind shields, both to minimize wind-related gauge undercatch. Even light winds can result in serious gauge undercatch of snowfall as demonstrated by Goodison (1978).

The 4.5 m s^{-1} transport speed was used for estimating arrival times of the AgI plume leading edge at each gauge. For sites off the plume axis a line perpendicular to the plume was used to estimate arrival times which are listed in Table 3. It is seen that arrival times for seeded gauges ranged between 0835 to 0910, or 35 to 70 min after start of seeding. RDJNC is the gauge near the junction of Highways 31 and 264. FARS and FARSE are the two most southerly gauges where S=south and SE=southeast. Other gauges are named by direction relative to sites shown on Fig. 1. For example, TARNW is northwest of TAR and DASNE is northeast of DAS.

Gauges are noted as seeded or nonseeded based on the AgI plume positions from both observations and model results to be discussed in Sec. 7. Four gauges were clearly crosswind of the AgI plume throughout the experiment, two north of the plume and two far south of the plume.

The two most southerly gauges (FARS and FARSE in Table 3) were effectively in a different weather regime as they received significantly less snow than all other Plateau top gauges. The aircraft scientist noted that cloud cover was more broken about 15 km south of the RRS-TAR area in the vicinity of gauges FARS and FARSE.

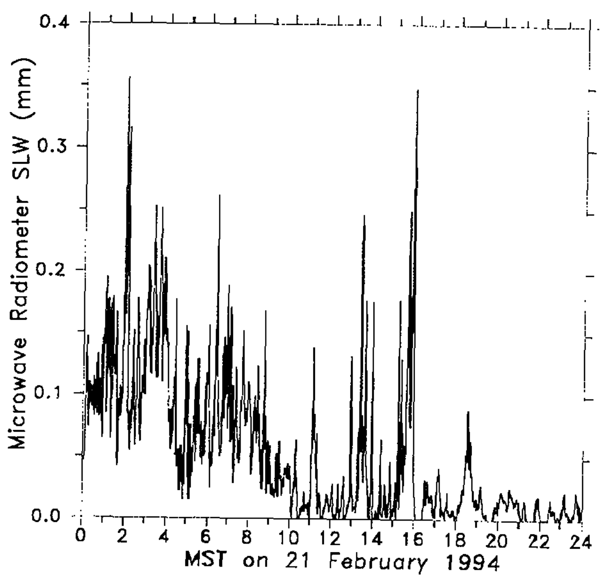

Fig. 6. Vertically-integrated SLW measured by the RRS microwave radiometer during 21 February 1994.

The AgI generator was turned off at 1215 because the storm was obviously ending and the cloud deck over the Plateau was breaking up. By 1230 the aircraft was beginning its final pass before returning to base. The last reference to observed snow in the van was at 1142 as it crossed the Plateau heading toward TAR. Later, after leaving TAR and driving along the upwind highway, the van encountered, "no plumes, no cloud (at the van altitude), no precipitation". The last visual report of any snowfall at the RRS was at 1200. The RRS log reported at 1246, "bright sunshine here, several large convective elements around."

Figure 6 shows that the vertically-integrated SLW over RRS gradually decreased after 0400 until about 1030 and was at low levels thereafter, with the exception of a few short-lived peaks characteristic of convective cell passage. Amounts of SLW were markedly greater during the several hours prior to seeding than during seeding, and likely as a consequence, precipitation decreased with time.

Since the storm was clearly ending by about 1200, precipitation accumulations were carefully extracted from the chart records with the aid of magnification for exactly 3.5 h after the estimated time of AgI plume arrival at (or crosswind of) each gauge. This placed the ending times between 1205 to 1240 and the resulting 3.5 h accumulations and equivalent hourly rates are listed in Table 3. In fact, snowfall had ended at all seeded gauges between 1100 to 1130. Nonseeded gauge TARNW again received snowfall from 1300 to 1320, with an accumulation of 0.38 mm. That brief episode likely was caused by a small convective shower as no other gauge detected snowfall at or near that time period.

Examination of the 3.5 h totals from Table 3, plotted on Fig. 1, suggests that seeding may have increased the snowfall at three of the four Plateau-top gauges under the AgI plume (DASNE, TARSW and TAR). These sites had somewhat more accumulation than RDJNC and TARNW, both north of the plume, each of which received 0.76 mm. Differences between these seeded and nonseeded gauges averaged 0.5 mm (0.02 inch), a limited amount over 3.5 h. Moreover, seeded gauges TARE and TARSE received less snowfall than DASNE or TARNW. The TARE observation might be anticipated because the gauge is on the Plateau's lee slope and so could be expected to be under subsiding, drying air. But there is no obvious reason why seeded gauge TARSE should have received so little snowfall. Consequently, it is possible but not certain that seeding increased the snowfall at a few gauges. However, any such increases were quite limited in magnitude in spite of the pronounced microphysical evidence of seeding from the aircraft and van 2D-C probes. Minor snowfall increases might be expected in view of the limited available SLW. The SW to NE gradient in total precipitation received by the seeded gauges is consistent with the indications of Fig. 4f. That gradient, and the 2D-C observations of aggregates along the upwind highway, suggest that most seeded snowfall reached the surface before the Plateau top's east edge, in agreement with the discussion of Sec. 5.

7. APPLICATION OF CLARK MESOSCALE MODEL

7.1 The Model and its Configuration

Although field observations were diverse and of high quality, their horizontal density was limited. Moreover, an approximately 600 m vertical layer

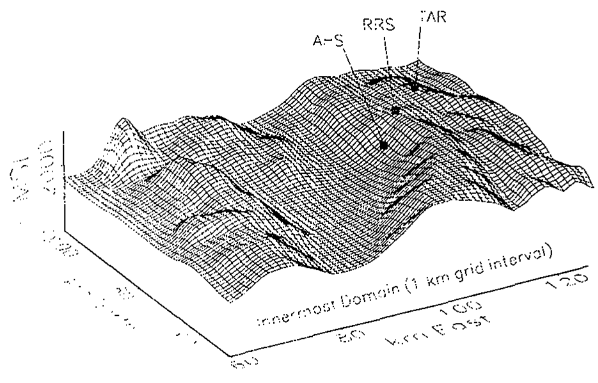

Fig. 7. Terrain for innermost domain used in the modeling. The vertical dimension has been exaggerated by a 9-to-1 factor.

above the Plateau top (300 m above highest terrain) could not be sampled because of aircraft safety considerations. Numerical modeling provides an opportunity to "fill in" the data sparse regions and to test application of treatment strategies.

The mesoscale model of Clark and associates of NCAR (Clark 1977, Clark and Farley 1984, Clark et al. 1994) was applied to this case study. The model is three dimensional and time dependent. The formulations are nonhydrostatic and anelastic, implying vertical accelerations are allowed, but the anelastic continuity equation is used to eliminate acoustic-scale waves. The model uses geo-spherical nonorthogonal coordinates with terrain following vertical coordinates such that the lowest grid points of the model are aligned with the terrain, and the top is at a constant level. For the application herein it was run in four dimensions, x, y, z and t, using three interactively nested domains to insure broader mesoscale patterns contributed to the fine-scale innermost resolution, while not exceeding computer resources. All the domains had a stretched vertical increment beginning with Δz = 100 m at the surface, increasing to Δz = 1 km by z = 18 km. The horizontal grids were 18 by 18, 30 by 30 and 66 by 54 for the outer, middle and innermost domains. The grid spacings of these domains were 9 km, 3 km, and 1 km respectively, and their time increments were 20, 10 and 5 s. Further details of the model setup as applied to the Plateau are given by Heimbach and Hall (1994).

Figure 7 depicts the terrain modeled for the innermost domain and shows the locations of AHS, RRS and TAR. The terrain has been twice run through a two dimensional nine-point smoother to insure computational stability. The gross features of the terrain have been captured; however, smaller canyons have been smoothed out.

"Warm cloud" microphysics are simulated using a modified form of the Kessler (1969) bulk parameterization. In this context warm cloud means unfrozen condensate which may be supercooled. The bulk parameterization assumes a Marshall-Palmer raindrop distribution. Condensation and evaporation are included. The ice microphysics are parameterized using the techniques of Koenig-Murray (Clark and Hall 1994, Bruintjes et al. 1994). There are two types of ice particles in this approach; those which are initially small and are produced by heterogeneous nucleation (type A), and those produced by freezing rain which are initially larger (type B). In the model, both types are allowed to be nucleated, grown by diffusion and accretion, and lost by sublimation and melting. The aggregation process is not included in the current version of the Clark model. Solar heating was not available in the version used.

The model was initialized using a sounding composited from Mount Pleasant (RAW) and Ely, NV, rawinsonde data, and aircraft observations. The 0900 RAW sounding had a saturated, nearly pseudoadiabatic layer between 803 and 695 mb. This layer became unsaturated by the 1100 RAW sounding. The 0500 Ely sounding likewise had a moist pseudoadiabatic layer. All the soundings had a surface inversion. The 0900 RAW sounding was used as a template for the initialization because this sounding was taken near the start of the experiment. The surface layer was changed from an inversion to a slightly stable lapse rate. The surface boundary layer winds were increased to 2 m s^{-1} and given a more westerly direction to reduce the sheltering influence of the Sanpete Valley. To incur computational stability, the last level of the composite sounding was repeated to 5 mb. The composite sounding is shown in Fig. 8.

The model was run on the NCAR CRAY-YMP computer. Job submission and graphics processing were done using workstations accessing the CRAY via the Internet. The model was run for one hour of simulated time with the warm cloud and ice options turned on for stabilization before tracer material was released. After one hour, the AHS AgI release was turned on at 22.5 gm hr^{-1} and the

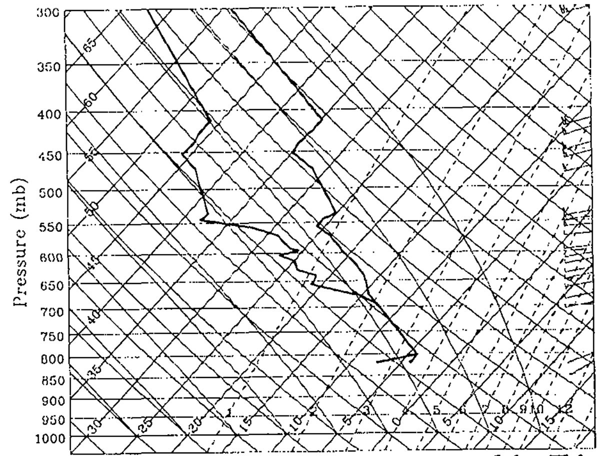

Fig. 8. Sounding used to initialize the model. This was composited from Ely, NV, and Mount Pleasant rawinsonde data, and aircraft data.

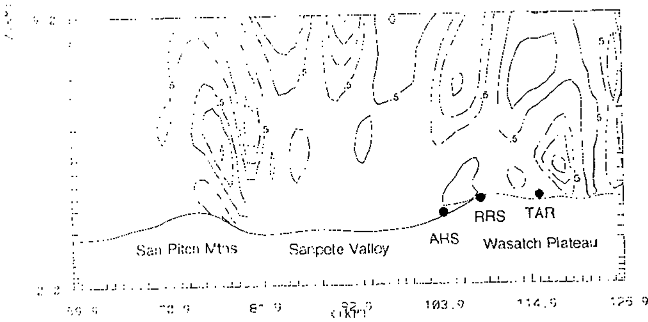

Fig. 9. West-to-east vertical cross section of vertical velocity after 3 h of simulated time. The north-south position of the cross section is approximately through AHS. The solid lines contour positive velocities and the broken lines are negative contours. The contour interval is 0.5 m s^{-1}.

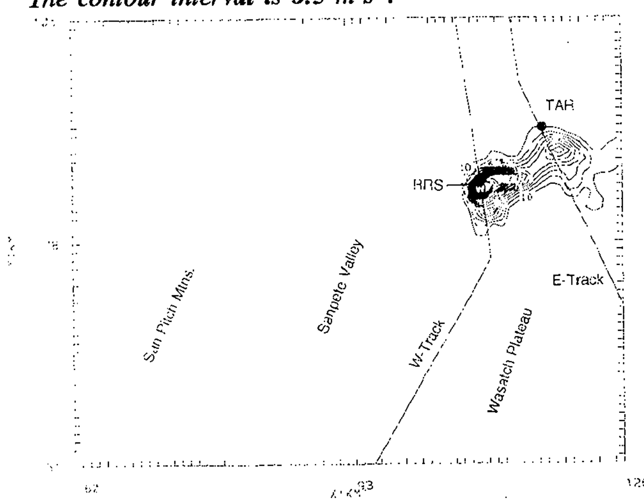

Fig. 10. Model estimates of AgI concentration at the 2.9 km altitude after a 2 h release from AHS. The minimum contour and contour interval are 10 pg m^{-3}.

model was run for an additional two hours. Approximately three hours of CPU time are needed for each hour of simulated time with this configuration.

7.2 Model Results

The model predicted little positive buoyancy at low levels over the Plateau (figure not included). Throughout the run there was negative buoyancy over the Plateau's western edge; that is, a generally stable atmosphere. The overall stable conditions suggest that vertical transport of the plumes was by mechanical means or perhaps by the gravity waves forcing weak convection at some locations. To the south and east outside the experimental area, some limited positive buoyancy was simulated. The initializing sounding was saturated-pseudoadiabatic throughout a deep layer which limited the opportunity for convection to develop within the model. As the upper levels dried out during the experiment, convection was more probable though only observed as weak shallow elements. Aircraft scientist voice notes reported intermittent in-cloud conditions at 3.7 km altitude.

The low level flow was weak and generally westerly throughout the simulation. Figure 9 is a west-to-east vertical cross section of vertical velocity, w, after 3 h of simulation. The cross section is at the 80 km mark in the model which runs approximately through AHS. Gravity waves are present but are weak and poorly organized over the Sanpete Valley due to the limited boundary layer wind speeds. The Rossby number, defined by,

$$R_o = \frac{U}{fL},$$

can be applied to confirm the type of wave motion excited by terrain (Steenburg and Mass 1994). U is the base state wind speed which for this case is on the order of 10 m s^{-1}. The half width of the terrain barrier, L, is approximately 10 km and f is the Coriolis parameter which is approximately 10^{-4} s^{-1}. This gives R_o a value larger than unity, making the Coriolis effect relatively small and giving gravity waves precedence over inertial waves assuming a stable domain is present. If R_o was less than unity, then Rossby waves would be generated.

Above approximately 5 km altitude, the vertical velocity becomes complicated with w having cores of alternating signs in a checker-board pattern. In this region the model predicted positive buoyancy, which would eliminate the gravity wave process. A secondary core of positive w is simulated over the vicinity of the eastern flight track and this is joined aloft with that over the western Plateau. Between these is a zone of $w < 0$ over the central portions of the Plateau.

The model-simulated AgI transport over the Plateau was weak until the plume reached sufficient altitude to become entrained in organized flow. This took approximately an hour after the start of release one hour into the simulation. Figure 10 is a horizontal depiction of the AgI plume at the 2.9 km level. The contours are in pico grams per cubic meter (10^{-12} g m^{-3}, hereafter pg m^{-3}). There are two centers of concentration. The western center is over the RRS while the eastern center is southeast of TAR with TAR just on the north edge of the simulated plume. Aircraft measurements indicated the AgI and SF_6 plumes were generally south of a line from RRS to TAR, in good agreement of the model's estimates. At the release point, weak surface winds and numerical diffusion combined to simulate an unrealistically wide lateral plume spread near the surface (figure not shown). Figure 11 is a south-north vertical cross section of the AgI plume which transects a point between AHS and RRS. It shows that in spite of negative buoyancy, an element of the AgI plume did ascend nearly 1 km above ground level. Some IN were detected above cloud tops implying that vertical IN transport did not rely entirely upon saturated processes.

The aircraft detected a strong IN plume at 3.9 km, but found none at 4.1 km. In Fig. 11, the smallest IN concentration contour (10 pg m^{-3}) reaches an elevation of 3.8 km. At 3.9 km, the model's estimated peak IN concentration was 10 pg m^{-3} (figure not shown). We assume the output of the DRI AgI generator was about 10^{16} IN gm^{-1} at -20°C. This is an order of magnitude more than at the coldest temperature sampled (-12°C) in a recent calibration of the DRI generator. This extrapolation is justified by comparing the DRI generator's calibration curve to that of other generators burning the same solution. This generator output combined with the model results implies 100 IN L^{-1} (at -20°C) are possible at 3.9 km. Using co-released SF_6 as an indicator of plume width, the aircraft required 28 s to cross the plume. The NCAR IN counter sample rate was 12.2 L min^{-1} and the total number of IN detected during that penetration was 272. Assuming a 10:1 cloud chamber loss results in 477 IN L^{-1}

effective at -20°C, the cloud chamber temperature. The model's estimate is approximately 20 percent of this calculated value. At the surface, the model predicted concentrations of AgI in excess of 100 pg m^{-3}. Converting this value as above gives surface concentrations in excess of 1000 L^{-1}. Values this high generally were not measured on the surface. The van data in the plume averaged 270 L^{-1}. However, large IN values were seen at TAR during the wind shift interval (average 948 L^{-1}) and for a 71-second part (average 1475 L^{-1}) of van pass 2 after the windshift started (both near Fig. 2 abscissa -37). While the plume was usually more dense at the surface on other dates, it appears to have been lifted during this study.

Figure 10 shows an AgI plume width of about 9 km at the Plateau top. This is in disagreement with the 2 to 5.5 km width actually measured at the lower aircraft and van levels and the 7 km width of the sheared tops along the eastern track (Fig. 2). The low wind speeds, long transport times and plume initialization procedures in the model are likely responsible for this difference. The actual plume (Fig. 4c) appears to have risen more rapidly and farther upwind from RRS than shown in Figs. 10 and 11. The secondary peak near TAR, however, is confirmed with the actual data in Fig. 4c. Actually, the case study measurements are the more unusual. The normal plumes over the Plateau on other dates appeared to hug the ground, be of higher concentration there, and were generally wider at Plateau top than at aircraft levels. As seen in Fig. 2, the aircraft level plume widths were the same as or wider than those measured by the van during this particular experiment.

The model predicted weak warm cloud processes over the Plateau which were forced by orography and gravity waves, while not being supported by buoyancy. Figure 12 depicts modeled cloud liquid water concentrations at 2.9 km after 3 h of simulated time. The occurrences are intermittent but are concentrated along the western edges of both the Plateau and the San Pitch Mountains. The major concentration southwest of RRS is in close agreement with the actual measurements shown in Fig. 2a. Both show a cloud of roughly 10 km size near the west track. Most aircraft passes did not explore the extent of the cloud upwind of RRS. Pass 14, flying along the plume from NE to SW, exited the cloud near the "approx. plume edge" position of Fig. 4. The LWC of 0.05 g m^{-3} in the 2 km zone upwind of the SF_6 plume was about twice that in

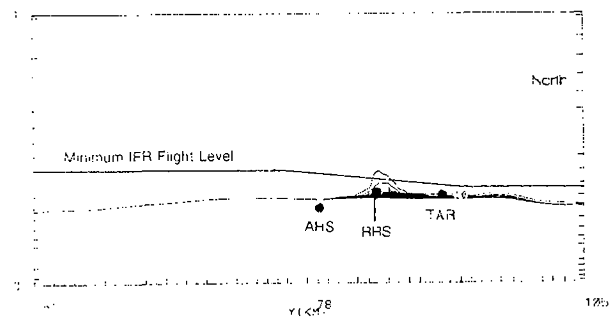

Fig. 11. AgI concentrations on a south-north vertical cross section through a point between AHS and RRS after 2 hr release time. The minimum contour and contour interval are 10 pg m^{-3}.

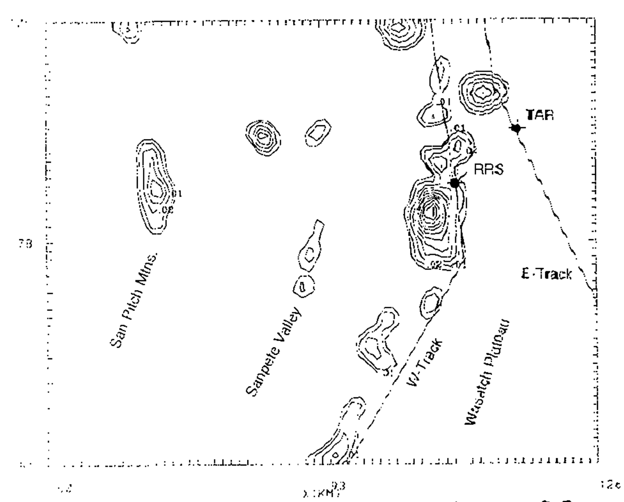

Fig. 12. Cloud liquid water concentrations at 2.9 km altitude after 3 hr simulated time. The minimum contour level and contour interval are 0.01 g m^{-3}.

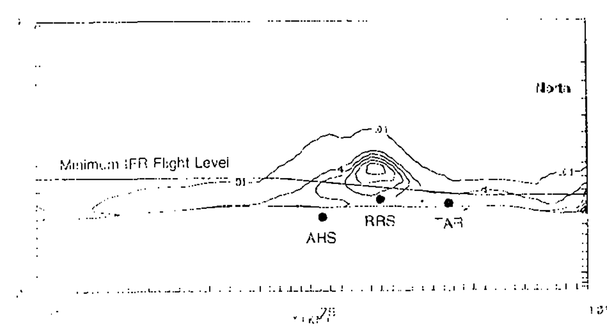

Fig. 13. Concentrations of small homogeneously-nucleated ice particles (Type A) on a south-north vertical cross section through a point between RRS and AHS. The contour interval is 4.0 L^{-1} and the 0.01 contour has also been drawn.

the adjacent plume. Perhaps the cloud was indeed more extensive upwind and wetter at earlier times in the day. The model-predicted intermittent occurrence of cloud elements is supported by aircraft scientist observations of, "in and out of clouds at 12.3 kft" (3.7 km). There are also several elements over the Sanpete Valley which are in response to weak gravity waves. A convective element was observed over the Sanpete Valley by the air crew.

In an analogous application of the Clark model to the Mogollon Rim in Arizona, Bruintjes et al. (1994) found complex flow and condensation patterns forced by orography and gravity waves. Likewise, Heimbach and Hall (1994) found complicated tracer and condensation patterns predicted by the model for a 1991 case on the Plateau. Both cited cases had stronger low-level winds and the gravity wave patterns were better organized than for the present case study. Although the present case had weak surface winds, gravity waves still appeared to be important for the vertical transport of seeding material and formation of condensation.

The model simulated ice formation within the warm cloud process. Figure 13 shows concentrations of ice type A (small heterogeneously nucleated crystals) on a south-north vertical cross section between AHS and RRS. The top of the ice is variable, as was the case for the warm cloud top, and the greatest ice elevation corresponds to that of the warm cloud top and peak vertical velocity. Type A ice was simulated in the vicinity of TAR, but higher concentrations were found to the south. Areas of type B ice occurrence were found by the model to be limited to zones in the vicinity of RRS and HAS (figure not shown).

8. SUMMARY AND CONCLUSIONS

The 21 February 1994 case was analyzed for plume characteristics including seeding responses for a single AgI plume co-released with SF_6 tracer gas well up the windward side of the Wasatch Plateau. The day was characterized by weak winds primarily from the southwest with weak convection enabling vertical transport of AgI to flight levels. The exposure of sites and mobile sampling platforms to the plume was estimated using a frame of reference which moved with the average wind. This enabled spatial and temporal coordination of multiple plume encounters, and allowed a uniform objective definition of nonseeded periods and locations. For the sampling aircraft, nonseeded portions of a flight path were 24 s flight intervals 12 s on either side of the co-released SF_6 plume. The nonseeded zones for the instrumented van were 2 km distances 1 km outside the SF_6 plume.

The plume was estimated to have been over particular ground sites for 4.25 h and to have generally moved from 235 degrees with a short period having a more southerly component. The angular plume width over the west flight track was estimated to have been 15 degrees with a brief wider period associated with a wind shift. Vertical plume transport to the Plateau top and to flight levels was rapid in the presence of limited horizontal wind speeds.

High concentrations of ice particles were associated with measured and predicted plumes at locations sampled by the van and aircraft. Ice particle concentrations and precipitation rates were enhanced, compared to nonseeded zones, by factors of about 10 for upwind highway van measurements, 40 for west track aircraft measurements, and variable amounts for east track aircraft passes. Ice water contents were always greater in the plume than in the nonseeded zones. Particle trajectories and concentration patterns indicated that most growth and precipitation occurred near the west track, where there was the most SLW available. Aggregation of high concentrations of ice particles appeared to be the mechanism for greater precipitation rates in the plume. Little snow was left to fall over the eastern ridge of the Plateau. Winds were atypically light during this experiment so that seeded snowfall for windier cases might be expected to settle further eastward.

Comparisons of precipitation totals between seeded and nonseeded gauges were suggestive that seeding may have produced a limited snowfall increase over period of the experiment of perhaps 0.5 mm at some gauges. However, one eastern seeded gauge received less snowfall than two nonseeded gauges also on top of the Plateau. Analyses of observations and physical reasoning suggest that most seeded snowfall settled to the Plateau top before crossing to its east edge, and perhaps before reaching the middle of the Plateau top at gauge TARSW. In retrospect, one or more gauges would have been useful along the upwind highway a few km north of RRS.

Updrafts predicted by the Clark model were associated with the windward edge of the Plateau and were generally limited to 0.5 m s^{-1} near the surface. There were areas of stronger down drafts over the Plateau, reaching speeds of -1.5 m s^{-1}. The complex gravity wave pattern forced a secondary maximum of tracer material several km south of TAR and some additional condensation over the northern portions of the eastern flight track.

The model suggests the case had weaker transport and diffusion of tracer material over the Plateau than indicated by field measurements. The plume transport time over the Plateau was slower than reality; however, the model ultimately simulated transport of AgI into liquid water cloud over the Plateau. The heights to which the simulated plumes were transported were in reasonable agreement with aircraft observations, but the simulated lateral spread was excessive at the surface. The model's smoothed terrain likely contributed to the less organized transport because the simulated canyons were shallow enough to limit the funneling of the poorly organized surface winds. The actual terrain consisted of a pronounced canyon downwind of AHS which likely limited crosswind horizontal dispersion within the canyon. The simulated clouds and ice were weak and shallow because buoyancy was not part of their formation. It is believed that buoyancy from solar heating did contribute to the observed clouds, and for that reason also contributed to a more vigorous vertical plume transport than was simulated. Overall, the model simulation produced a reasonable first-approximation of reality.

In summary, AgI seeding during this experiment produced strong microphysical evidence of markedly enhanced ice particle concentrations on the Plateau top and at aircraft levels. Plumes released on the windward slope were readily transported over the Plateau in spite of limited horizontal winds. Plume widths were limited, suggesting seeding generators at similar high altitude sites should be spaced no more than 5 km crosswind. Horizontal dispersion from other high altitude sites could be more or less than from AHS depending upon local topography.

Seeding apparently increased the snowfall, especially on the western portion of the Plateau top, but accumulations were limited. Seeding appeared to significantly increase the aggregation of snowflakes along the upwind highway. Best estimates of snowfall rates caused by seeding are 0.4 mm h^{-1} based on 2D-C estimates along the upwind highway (Table 2), and less than half that rate from gauges on the central and eastern portions of the Plateau top (Sec. 6). Of course, SLW amounts were quite limited during this weak and diminishing final portion of the storm, so seeding potential would be expected to be quite limited as well.

Overall, the results of this experiment are in general agreement with current physical understanding of how winter orographic seeding should work.

Acknowledgments

Many individuals contributed to the success of the 1994 Wasatch Plateau field program. Notable among them are Clark Ogden, Erick Faatz, Dennis Faatz and Barry Saunders of the Utah Division of Water Resources; Dennis Wellman and Stan Wilkison of NOAA; Arlen Huggins and Melanie Wetzel of the Desert Research Institute; Glenn Cascino, Jack McPartland, Arlen Hilton and Roger Hansen of the Bureau of Reclamation; and Bill Hauze of North American Weather Consultants. Gerhard Langer checked the field operation of the NCAR IN counter. Terry Clark and Bill Hall of NCAR provided generous help in adapting their numerical model to the Utah program and in interpreting the results. This applied research was primarily funded by the Utah/NOAA AMP in cooperation with the Utah Division of Water Resources. Various equipment resources were supplied by the Bureau of Reclamation, and CRAY-YMP computer time was provided by NCAR which is partly funded by the National Science Foundation. The reviewers are thanked for their many helpful comments which improved this paper.

9. REFERENCES

Benner, R.L. and R. Lamb, 1985: A fast response continuous analyzer for halogenated atmospheric tracers. *J. Atmos. Oceanic Tech.*, **2**, 582-589.

Bruintjes, R.T., T.L. Clark and W.D. Hall, 1994: Interactions between topographic air flow and cloud precipitation developing during the passage of a winter storm in Arizona. *J. Appl. Meteor.*, **51**, 48-67.

Clark, T.L., 1977: A small scale dynamic model using terrain following coordinate transformation. *J. Comp. Physics*, **24**, 186-215.

__________ and R.D. Farley, 1984: Severe downslope windstorm calculations in two and three spatial dimensions using anelastic interactive grid nesting: a possible mechanism for gustiness. *J. Atmos. Sci.*, **41**, 329-350.

__________, W.D. Hall and R.M. Banta, 1994: Two- and three-dimensional simulations of the 9 January 1989 severe Boulder windstorm: comparison with observations. *J. Atmos. Sci.*, **51**, 2317-2343.

DeMott, P.J., A.B. Super, G. Langer, D.C. Rogers, and J.T. McPartland, 1995: Comparative characterizations of the ice nucleus ability of AgI aerosols by three methods. *J. Wea. Mod.*, **27**, in press.

Deshler, T.D. and D.W. Reynolds, 1990: The persistence of seeding effects in a winter orographic cloud seeded with silver iodide burned in acetone. *J. Appl. Meteor.*, **29**, 477-488.

__________, __________, and A.W. Huggins, 1990: Physical response of winter orographic clouds over the Sierra Nevada to airborne seeding using dry ice or silver iodide. *J. Appl. Meteor.*, **29**, 288-330.

Finnegan, W.G. and R.L. Pitter, 1988: Rapid ice nucleation by acetone-silver iodide generator aerosols. *J. Wea. Mod.*, **20**, 51-53.

Griffith, D.A., J.R. Thompson and D.A. Risch, 1991: A winter cloud seeding program in Utah. *J. Wea. Mod.*, **23**, 27-34.

Goodison, B.E., 1978: Accuracy of Canadian snow gage measurements. *J. Appl. Meteor.*, **17**, 1542-1548.

Heimbach, J.A. and A.B. Super, 1988: The Bridger Range, Montana, 1986-1987 snow pack augmentation program. *J. Wea. Mod.*, **20**, 19-26.

__________ and W.D. Hall, 1994: Applications of the Clark Model to winter storms over the Wasatch Plateau. *J. Wea. Mod.*, **26**, 1-11.

Heymsfield, A.J., 1986: Aggregates as embryos in seeded clouds. *Precipitation Enhancement-A Scientific Challenge, Meteor. Monogr.*, No. 43, Amer. Meteor. Soc, 33-41.

Hogg, D.C., F.O. Guiraud, J.B. Snider, M.T. Decker and E.R. Westwater, 1983: A steerable dual-channel microwave radiometer for measurements of water vapor and liquid in the troposphere. *J. Climate Appl. Meteor.*, **22**, 789-806.

Holroyd, E.W., 1987: Some techniques and uses of 2D-C habit classification software for snow particles. *J. Atmos. Ocean. Tech.*, **4**, 498-511.

__________ and J.E. Jiusto, 1971: Snowfall from a heavily seeded cloud. *J. Appl. Meteor.*, **10**, 266-269.

__________, J.T. McPartland and A.B. Super, 1988: Observations of silver iodide plumes over the Grand Mesa of Colorado. *J. Appl. Meteor.*, **27**, 1125-1144.

Huggins, A.W., 1994: *Final report; Desert Research Institute Field Operations 1994 NOAA/UTAH Field Program*. Reno, NV. 77pp.

__________, 1995: Mobile microwave radiometer observations: Spatial characteristics of supercooled cloud water and cloud seeding implications. *J. Appl. Meteor.*, **34**, 432-446.

Kessler, E., 1969: On the distribution and continuity of water substance in atmospheric circulations. *Meteor. Monogr.*, No. 32, Amer. Meteor. Soc., 94pp

Langer, G., 1973: Evaluation of NCAR ice nuclei counter. Part I: Basic operations. *J. Appl. Meteor.*, **10**, 1000-1011.

Steenburg, W.J. and M.J. Mass, 1994: The structure and evolution of a simulated Rocky Mountain lee trough. *Mon. Wea. Rev.*, **122**, 2740-2761.

Super, A.B., 1994: Implications of early 1991 observations of supercooled liquid water, precipitation and silver iodide on Utah's Wasatch Plateau. *J. Wea. Mod.*, **26**, 19-32.

__________, 1995: Case studies of microphysical responses to valley-released operational AgI seeding of the Wasatch Plateau, Utah. *J. Wea. Mod.*, **27**, in press.

Super, A.B. and B.A. Boe, 1988: Microphysical effects of wintertime cloud seeding with silver iodide over the Rocky Mountains. Part III: Observations over the Grand Mesa, Colorado. *J. Appl. Meteor.*, **27**, 1166-1182.

__________, __________, E.W. Holroyd and J.A. Heimbach, 1988: Microphysical effects of wintertime cloud seeding with silver iodide over the Rocky Mountains. Part I: Experimental design and instrumentation. *J. Appl. Meteor.*, **27**, 1145-1151.

__________ and J.A. Heimbach, 1983: Evaluation of the Bridger Range winter cloud seeding experiment using control gages. *J. Climate Appl. Meteor.*, **22**, 1989-2011.

__________ and __________, 1988: Microphysical effects of wintertime cloud seeding with silver iodide over the Rocky Mountains. Part II: Observations over the Bridger Range, Montana. *J. Appl. Meteor.*, **27**, 1152-1165.

__________ and E.W. Holroyd, 1994: Estimation of effective AgI ice nuclei by two methods compared with measured ice particle concentrations in seeded orographic cloud. *J. Wea. Mod.*, **26**, 33-40.